
Since January 2020 Elsevier has created a COVID-19 resource centre with free information in English and Mandarin on the novel coronavirus COVID-19. The COVID-19 resource centre is hosted on Elsevier Connect, the company's public news and information website.

Journal of Hazardous Materials 430 (2022) 128414

Contents lists available at ScienceDirect

Journal of Hazardous Materials

journal homepage: www.elsevier.com/locate/jhazmat

Research Paper

# Efficient disinfection of SARS-CoV-2-like coronavirus, pseudotyped SARS-CoV-2 and other coronaviruses using cold plasma induces spike protein damage

Hongbo Qin [a,b,1], Hengju Qiu [a,1], Shi-Ting He [b,1], Bixia Hong [b,1], Ke Liu [b,1], Fuxing Lou [b], Maochen Li [b], Pan Hu [a], Xianghao Kong [a], Yujie Song [a], Yuchen Liu [a], Mingfang Pu [b], Pengjun Han [b], Mengzhe Li [b], Xiaoping An [b], Lihua Song [b], Yigang Tong [b,c,*], Huahao Fan [b,**], Ruixue Wang [a,**]

[a] College of Mechanical and Electrical Engineering, Beijing University of Chemical Technology, Beijing 100029, China
[b] College of Life Science and Technology, Beijing University of Chemical Technology, Beijing 100029, China
[c] Beijing Advanced Innovation Center for Soft Matter Science and Engineering, Beijing University of Chemical Technology, Beijing 100029, China

## HIGHLIGHTS

- Wide-spectrum disinfection using pulse power-driven CAP on coronavirus and SARS-CoV-2 variants is studied for the first time.
- CAP effectively disinfects coronavirus and SARS-CoV-2 variants within 300s.
- The oxidative reaction of CAP affects the SARS-CoV-2 spike protein rather than damaging viral RNA.
- The disinfection effect of RONS on coronavirus follows the order of $ONOO^-$ > $O_2^-$>$^1O_2$ > ·OH.

## GRAPHICAL ABSTRACT

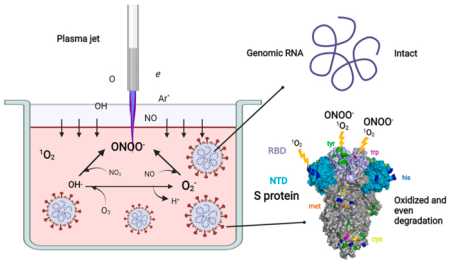


## ARTICLE INFO

Editor: Danmeng Shuai

*Keywords:*
SARS-CoV-2
Cold pressure plasma
Pseudotyped variants
Coronavirus
Short-lived reactive species
Peroxynitrite anion

## ABSTRACT

Coronavirus disease 2019 (COVID-19) has become a worldwide public health emergency, and the high transmission of SARS-CoV-2 variants has raised serious concerns. Efficient disinfection methods are crucial for the prevention of viral transmission. Herein, pulse power-driven cold atmospheric plasma (CAP), a novel sterilization strategy, was found to potently inactivate SARS-CoV-2-like coronavirus GX_P2V, six strains of major epidemic SARS-CoV-2 variants and even swine coronavirus PEDV and SADS-CoV within 300 s (with inhibition rate more than 99%). We identified four dominant short-lived reactive species, $ONOO^-$, $^1O_2$, $O_2^-$ and·OH, generated in response to CAP and distinguished their roles in the inactivation of GX_P2V and SARS-CoV-2 spike protein receptor binding domain (RBD), which is responsible for recognition and binding to human angiotensin-converting enzyme 2 (hACE2). Our study provides detailed evidence of a novel surface disinfection strategy for SARS-CoV-2 and other coronaviruses.

* Corresponding author at: College of Life Science and Technology, Beijing University of Chemical Technology, Beijing 100029, China.
** Corresponding authors.
*E-mail addresses:* tong.yigang@gmail.com (Y. Tong), fanhuahao@mail.buct.edu.cn (H. Fan), wrx@mail.buct.edu.cn (R. Wang).
[1] These authors contributed equally.

https://doi.org/10.1016/j.jhazmat.2022.128414
Received 11 December 2021; Received in revised form 19 January 2022; Accepted 31 January 2022
Available online 4 February 2022

## 1. Introduction

Severe acute respiratory syndrome coronavirus 2 (SARS-CoV-2) is a novel coronavirus that emerged in 2019 and caused the global epidemic of COVID-19 (Dehning et al., 2020; Zhou et al., 2020). It is infectious to the human respiratory tract, causing fever, dry cough, fatigue, shortness of breath, body aches, diarrhea, and other symptoms (Latinne et al., 2020). With viral evolution, several variants, such as B.1.1.529 (Omicron), B.1.617.2 (Delta), B.1.351 (Beta) and P.1 lineage (Gamma), have emerged and become the dominant strains in the pandemic, likely facilitating transmission in the population, increasing the severity of infection and diminishing vaccine efficacy (Fan et al., 2022; Li et al., 2021a,b, 2022; Lou et al., 2021). There is an urgent need to develop additional prevention and treatment strategies and methods against SARS-CoV-2.

It has been reported that SARS-CoV-2 can survive and retain infectious on the surface of substances for up to 9 days, therefore, effective disinfection strategies are vital for preventing and minimizing the virus transmission (Kampf et al., 2020; Noorimotlagh et al., 2021). Current surface disinfection methods include ultraviolet disinfection, ozone disinfection, heat sterilization and chemical agent disinfection (Heilingloh et al., 2020; Hijnen et al., 2006; Wu et al., 2020; Xiling et al., 2021). Limitations of these disinfection methods include irreversible harm to humans or environmental contamination. Cold atmospheric plasma (CAP), having advantages of low cost, high flexibility and great safety, is recognized as a new hope for viral disinfection (Zhang et al., 2021; Bernhardt et al., 2019; Criscuolo et al., 2021; Song et al., 2022; Tx et al., 2020; Vilcassim et al., 2021; Walcher et al., 2021).

CAP generates complex mixtures of reactive substances, such as reactive oxygen and nitrogen species (RONS). Considering its distinct characteristics compared to neutral gas, plasma is regarded as one of the four states of matter together with solid, liquid and gas (Filipić et al., 2021). During the past two decades, plasma has attracted great attention in the food production industry and biomedical field such as oncotherapy and skin lesions recovery, which affirm the safety for its application (Bourke et al., 2018; Chen et al., 2017; Li et al., 2019; Metelmann et al., 2012). Previous studies have reported that bacteria, including *Staphylococcus aureus* and *Bacillus atrophaeus*, can be successfully inactivated in vitro and in vivo using CAP (Keudell et al., 2010; Nicol McKayla et al., 2020; Zhang et al., 2016). In addition to bacteria, plasma exhibits a disinfecting effect on bacteriophages and feline calicivirus (Aboubakr et al., 2015; Guo et al., 2018; Sakudo et al., 2019). The inactivation of SARS-CoV-2 by CAP was first demonstrated by Chen et al., who used CAP to inactivate SARS-CoV-2 on various surfaces (Chen et al., 2020), and their alternative current (AC)-powered plasma exhibited efficient disinfection of virus within 180 s with SARS-CoV-2 at $2 \times 10^5$ PFU/mL in a 25 μL volume. Guo et al. proposed another strategy to inactivate SARS-CoV-2 pseudovirus using plasma-activated water (PAW) which can be generated in large volume and remains effective for several days, and disinfection of SARS-CoV-2 was achieved using PAW treatment for 5–10 min (Guo et al., 2021).

SARS-CoV-2 is classified as a biosafety level 3 (BSL-3) agent, which impedes related research. Lam et al. reported that pangolin coronavirus GX_P2V isolated from Manis javanica exhibited high genomic similarity, sharing 92.2% amino acid identity with the SARS-CoV-2 spike protein (S protein), and using the same receptor with SARS-CoV-2 to initiate infection (Fan et al., 2020a; Hu et al., 2021; Lam et al., 2020). Fan et al. employed the GX_P2V model for SARS-CoV-2 pharmaceutical research and successfully screened cepharanthine from two libraries of 2406 clinically approved drugs, which has been verified by other research groups (Drayman et al., 2021; Fan et al., 2020b; Li et al., 2021b; Ohashi et al., 2021). Pei et al. used the GX_P2V model to screen ultrashort peptide RBD inhibitors that combined with hACE2 (Pei et al., 2021). All of these cases demonstrate that pangolin coronavirus GX_P2V is an ideal substitute model for SARS-CoV-2 research. Furthermore, pseudoviruses expressing the S protein can be introduced to study the entry stage of SARS-CoV-2.

In this study, SARS-CoV-2-like coronavirus GX_P2V, pseudoviruses incorporated with SARS-CoV-2 variants S protein were utilized to examine the disinfection efficacy of CAP (Fig. 1A). In addition, two other important porcine coronaviruses, coronavirus porcine epidemic diarrhea virus (PEDV) and swine acute diarrhea syndrome coronavirus (SADS-CoV) were employed to evaluate the disinfection ability of CAP on coronavirus. Microscopy images, viral attachment assays, enzyme-linked immunosorbent assays (ELISAs), sodium dodecyl sulfate polyacrylamide gel electrophoresis (SDS–PAGE) assays, and viral RNA detection and scavenger addition assays were performed to investigate the disinfection mechanisms of CAP on coronavirus and to distinguish the roles of RONS generated using plasma jets.

## 2. Materials and methods

### 2.1. CAP fabrication and characterization

The CAP was constructed in plasma jet form, in which the plasma plume was ejected from the nozzle. This construction is easy to carry and suitable for surface treatment. The CAP device was placed 10 mm above the solution. The treatment area can be adjusted simply by grouping individual plasma jets together (Wang et al., 2017). A schematic diagram of the experimental device is shown in Fig. 1B. The plasma jet adopted a typical needle-ring electrode structure, and the specific structure was shown previously (Wang et al., 2016a, 2016b). The hollow stainless steel tube was inserted into the quartz tube (inner diameter 1.5 mm, wall thickness 0.1 mm, length 150 mm) as the high voltage electrode. A copper strip with a width of 10 mm and a thickness of 180 mm was wrapped on the surface of the quartz tube as the grounding electrode. The plasma jet was powered using a pulse power supply (Xi'an Smart Maple Electronic Technology, HVP-22 P, Xi'an, China). The working gas was research grade argon (99.999%) with a flow rate of 2 SLM (standard liter per minute). The voltage and current characteristics were monitored using a high voltage probe (Tektronix, P6015A, 1000:1, OR, USA) and a current probe (Pearson, Model 4100, 1 V/A) via a digital oscilloscope (Lecory WR204XI, NYC, USA), respectively. Using an applied voltage of 8 kV, two current peaks were observed at the rise and fall times of the voltage waveform (Fig. S1(A)), presenting a typical dielectric barrier discharge (DBD) character. The pulse power supply with a narrow pulse rise and fall time provided a high instantaneous power of 9 kW, and the average discharge power was calculated as 10.89 W (Fig. S1(B)).

The fiber optic cable was placed at the exit nozzle of the plasma jet with a spacing of 40 mm to capture the light emitted from the plasma jet to the spectrometer (Fuxiang, FX2000, Shanghai, China). A thermocouple (Chenyi, CY-009, Hangzhou, China) was used to measure the plate wall temperature after plasma jet treatment.

### 2.2. Virus and cell proliferation

African green monkey kidney (Vero E6) cells and human hepatoma carcinoma cell Huh 7 obtained from American Type Culture Collection (ATCC, Manassas, VA, USA) were maintained in Dulbecco's modified Eagle's medium (DMEM, HyClone, Utah, USA) supplemented with 10% fetal bovine serum (FBS), 1% nonessential amino acids (NEAAs) and a 1% antibiotic-antimycotic mixture (Gibco, NY, USA). The SARS-CoV-2-related pangolin coronavirus GX_P2V (accession No. MT072864.1) was isolated from smuggled dead Manis javanica in 2017, and it was propagated in Vero E6 cells. PEDV and SADS-CoV were maintained and amplified in Huh 7 cells. The cells and virus were cultured at 37 °C in a 5% $CO_2$ incubator.

### 2.3. Detection of the virucidal effect using 50% tissue culture infectious doses (TCID50) and plaque assays

To determine the virucidal effect of CAP on coronavirus, TCID50 assays and plaque assays were performed to determine the infectivity of CAP-treated versus untreated viruses as previously described (Weston et al., 2020). Three species of coronavirus GX_P2V ($2 \times 10^5$ PFU/mL), PEDV ($1 \times 10^5$ PFU/mL) and SADS-CoV ($1 \times 10^5$ PFU/mL) suspended in DMEM were subjected to CAP or Ar jet for various durations (10 s, 30 s, 60 s, 120 s, 180 s and 300 s). After CAP or Ar (without plasma) treatments, viruses were serially diluted in DMEM containing 10% FBS, and then the dilutions (100 μL) were inoculated into 96-well plates pre-seeded with cell monolayers in duplicate. The cells were incubated at 37 °C with 5% $CO_2$ and observed daily for cytopathic effect (CPE) development for up to 3 days. The CPE of each well was observed and recorded for TCID50 determination. The titers of infectious viruses are expressed as log10 TCID50/mL. For the plaque assay, viruses ($2 \times 10^5$ PFU/mL) treated with CAP or Ar were diluted 10-fold from $10^{-1}$ to $10^{-6}$ in DMEM containing 10% FBS (Fan et al., 2020b). One milliliter of each dilution was introduced into a 6-well plate preseeded with cell monolayers for a 2 h incubation at 37 ℃ with 5% $CO_2$. The virus inoculum was completely removed, and the cells were supplemented with culture media. The cells were examined daily for CPE up to 3 days. Cells were fixed in 4% paraformaldehyde for 2 h and then stained with crystal violet for 10 min. The plaques were quantified after crystal violet staining and washing with water.

### 2.4. Inactivation assay of pseudotyped SARS-CoV-2 variants

The SARS-CoV-2 S protein pseudotyped variants were prepared using a VSV pseudotyped virus packaging system, and the packing and quantification procedures were based on the protocol published by Nie

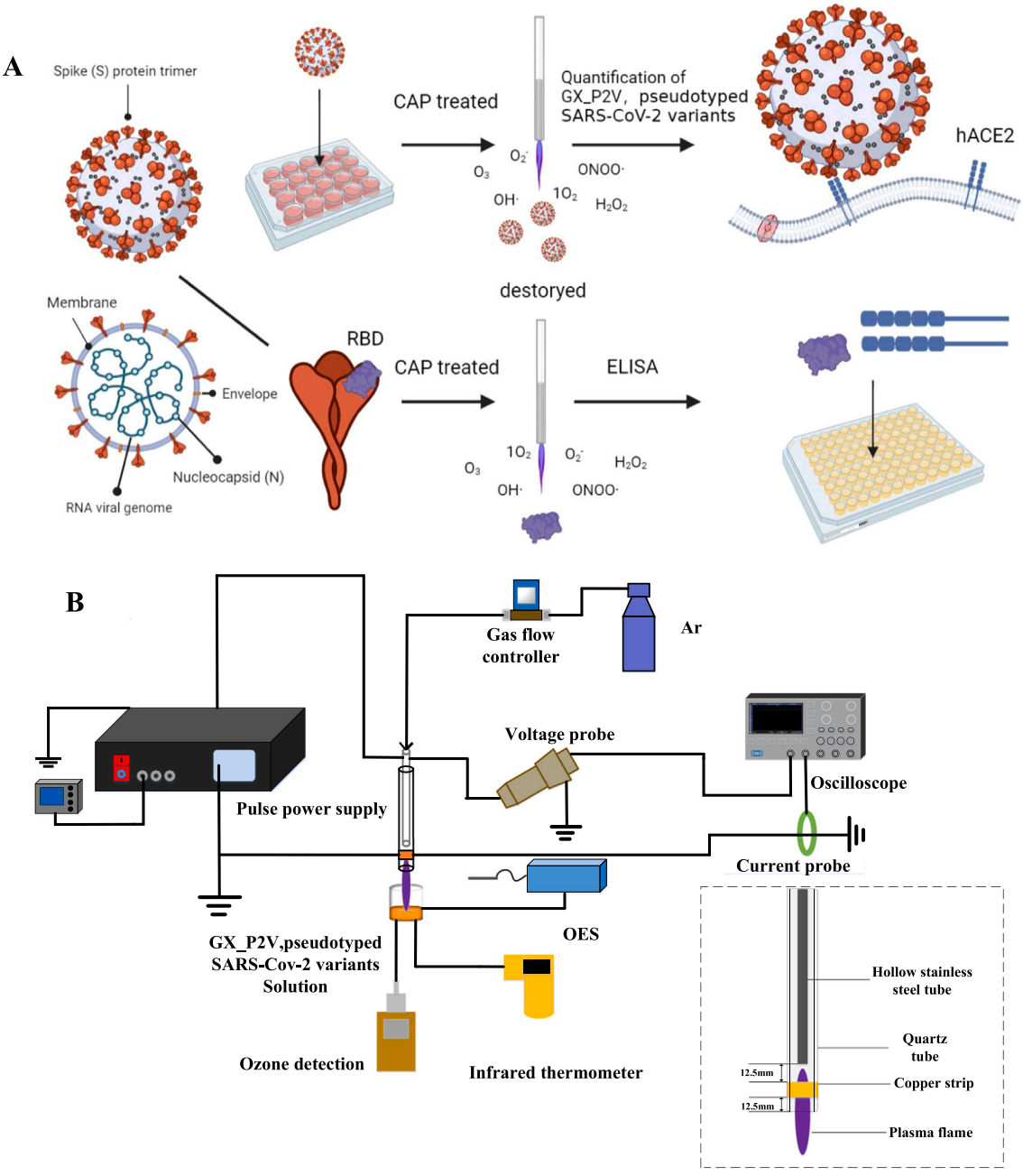


**Fig. 1.** Schematic diagrams. (A) Schematic diagram of virus inactivation. (B) Schematic diagram of the plasma jet device for virus treatment.

et al. (Nie et al., 2020). Plasmids expressing various S protein variants of SARS-CoV-2 were synthesized by Ruibo Xingke Biotech (Beijing, China). HEK-293 T cells were obtained from ATCC. One hundred microliters of pseudoviruses bearing wild type or variant S protein treated with CAP and untreated pseudovirions were diluted 10-fold and mixed with a 9-fold volume of DMEM supplemented with 10% fetal bovine serum (FBS), 1% nonessential amino acids (NEAAs) and a 1% antibiotic-antimycoticen mixture (Gibco, NY, USA) and 100 μL Vero E6 cells. After incubation at 37 ℃ and 5% $CO_2$ for 24 h, then the luciferase substrate was added for chemiluminescence detection. To determine the disinfection ability of CAP, the relative light unit (RLU) of pseudovirus-containing medium was measured using a microplate reader (Bio Tek, H1), and the inactivation effect was calculated as follows:

$$Inhibition \quad (\%) = 1 - \frac{RLU(CAP-treated) - RLU(blank)}{RLU(CAP-untreated) - RLU(blank)} \times 100\%$$

### 2.5. Transmission electron microscopy (TEM)

Transmission electron microscopy (TEM) was performed to determine the morphological characteristics of virus before and after CAP treatment. One hundred microliters of concentrated GX_P2V particles ($10^7$ PFU/mL) was subjected to CAP for 180 s. The virus samples were irradiated with ultraviolet light for 50 min to ensure the safety for subsequent analysis. Twenty microliters of untreated or treated GX_P2V suspension was pipetted onto carbon-coated support membrane copper mesh and retained for 10 min at 20 ℃, followed by negative staining with 2% phosphotungstic acid solution and for 1 min retention. After further drying, virus particles were observed under an electron microscope (JEM-1200EX, Japan) at an accelerating voltage of 100 kV.

### 2.6. Detection of viral attachment

GX_P2V treated with CAP was added to 24-well plates preseeded with Vero E6 cells and incubated for 2 h at 4 ℃ (for viral attachment) and 37 ℃ (for viral attachment and entry). After functional GX_P2V attachment to cells, the unbound GX_P2V was removed, and the cells were washed with PBS 3 times before collection for subsequent real-time polymerase chain reaction (RT–qPCR) analysis.

After harvesting the cells, total viral RNA was extracted and purified using a Flying Shark® Tissue & Cell RNA Kit (Cat No. RNE11, Nobelab Biotech, Beijing, China) and AxyPrep™ Body Fluid Viral DNA RNA Kit (LOT. 05921KC5, Corning Life Science, Wujiang, China) in accordance with the manufacturer's instructions. Reverse transcription was performed using a Hifair II 1st Strand cDNA Synthesis Kit (Yeasen Biotech, Shanghai, China) to obtain viral cDNA. To perform the RT–qPCR assay, 1 μL viral cDNA was mixed with 10 μL Hieff qPCR SYBR Green Master Mix, 0.4 μL forward primer, 0.4 μL reverse primer and 8.2 μL water. RT–qPCR was performed using a QuantStudio 1 Real-Time PCR detection system (Applied Biosystems, CA, USA) with a two-stage SYBR Green method. Primer sequences are listed in Table S1 and have been previously described (Pei et al., 2021), and the procedure was performed as follows: 95 ℃ for 10 min; 40 cycles of 95 ℃ for 10 s and 60 ℃ for 30 s; and melting curve stage: 95 ℃ for 15 s, then 60 ℃ for 1 min and 95 ℃ for 1 s

### 2.7. Effect of CAP on SARS-CoV-2 RBD protein

The RBD located at the top side of the S protein is the key component for cellular entry of SARS-CoV-2. To investigate the effect of CAP on the SARS-CoV-2 RBD, ELISA was employed. ELISA of the RBD treated with CAP was performed using a SARS-CoV-2 (2019-nCoV) Inhibitor Screening ELISA Kit (Sino Biological, Cat No. KIT001A, Beijing, China). Briefly, RBD (horseradish peroxidase [HRP]-conjugated) (150 ng/mL) treated with CAP for different durations was added to each well and incubated at room temperature for 1 h. The wells were subsequently washed and incubated with 3,3′,5,5′-tetramethylbenzidine (TMB) substrate for 15 min in the dark. Then, stop solution was added, and the absorbance of each well was measured at 450 nm using a microplate reader (Bio Tek, H1).

### 2.8. SDS-polyacrylamide gel electrophoresis (PAGE) of SARS-CoV-2 RBD

Purified SARS-CoV-2 RBD (2 μg/mL) was treated with Ar-fed CAP for various durations. The proteins were boiled at 100 ℃ for 10 min and loaded in 15% gradient SDS–PAGE gels. Finally, the RBD band was visualized using Coomassie Blue staining.

### 2.9. Investigation of the CAP degradation effect on viral RNA

GX_P2V particles were exposed to Ar-fed CAP for various durations. Then, genomic RNA was extracted and subjected to reverse transcription to obtain complementary DNA (cDNA). Specific primers of which amplification product covers the region from nucleotide 24025–24145 were employed to amplify the genomic region of the S protein in RT–qPCR analysis. The results are shown as the copy number of viral RNA.

### 2.10. Measurement of RONS in CAP

CAP-generated RONS in the liquid phase were measured using different assay kits. The·OH generated by the CAP device was measured. Terephthalic acid is a well-known specific probe for detecting·OH due to its high reaction rate coefficient ($k = 4.3 \times 10^9\ M^{-1}\ s^{-1}$) (Kanazawa et al., 2011). The generation of hydroxyterephthalic acid was measured using a microplate reader according to the fluorescence intensity (excitation wavelength 310 nm, emission spectrum 420 nm). Furfuryl alcohol is extremely reactive to $^1O_2$ ($k = 1.2 \times 10^8\ M^{-1}\ s^{-1}$) (Cote et al., 2018). A high-performance liquid chromatography system was used to analyze the decay of furfuryl alcohol. The concentration used for detection was 1 mM, and the degradation rate of furfuryl alcohol represented the yield of $^1O_2$. A superoxide anion detection kit (R30343–50 T,Yuanye Bio-Technology,Shanghai, China) was used to detect superoxide anion radicals ($O_2^-$) in solution by hydroxylamine oxidation. $O_2^-$ reacts with hydroxylamine to form $NO_2^-$, $NO_2^-$ reacts with aminobenzene sulfonic acid and naphthylamine to form pink P-benzenesulfonic acid-naphthylamine, and the absorbance at 530 nm was determined using a microplate reader. The color of $O_2^-$ was proportional to the color within a certain range. The peroxynitrite anion ($ONOO^-$) content of liquid samples was detected using an $ONOO^-$ detection kit (MM-0798M1,MEIMIAN,Yancheng, China). The O56 reactive oxygen species probe in the kit reacts with $ONOO^-$ to form green fluorescent substances, which had a maximum excitation/emission wavelength of 488/516 nm and were detected using a microplate reader.

### 2.11. Scavenger addition assay

To further verify the role of active substances generated by plasma in virus inactivation, 0.1 M D-mannitol (MI828–500 g, Jiuding chemistry, China), 0.05 M L-histidine (H-25672, HEOWNS, China), 100 U/mL superoxide dismutase (S8410, Solarbio, China) and 1 mM ebselen (QE417–10 mg,Jiuding Chemistry, China) were employed to quench·OH, $^1O_2$ and·OH, $O_2^-$ and $ONOO^-$, respectively. The scavenger solution was added to the viral suspension prior to CAP treatment. A viral suspension without scavenger treated with CAP was used as a control. All CAP-treated samples were subjected to plasma jet treatment for 180 s. By comparing the titers of the CAP-treated virus to virus treated with scavenger and then CAP, the roles that each active substance played were clarified. In addition, titers of virus suspension treated with scavenger were measured to exclude the effect of D-Man, L-His and SOD on viruses and cells.

## 3. Results

### 3.1. Disinfection of SARS-CoV-2-like pangolin coronavirus GX_P2V by CAP

In this study, pangolin coronavirus GX_P2V, which shares 92.2% amino acid identity with the SARS-CoV-2 S protein, was employed as a model to study the disinfection effect of Ar-fed CAP on SARS-CoV-2. Vero E6 cells were used as recipient cells for the assessment of CAP's disinfection effect. First, different volumes of viral suspensions ($2 \times 10^5$ PFU/mL) were exposed to Ar-fed CAP for 300 s. The disinfection effect of CAP on infectious virus increased as virus volume decreased (Fig. 2A). Then, 100 μL virus suspensions were subjected to Ar-fed CAP for various durations. Meanwhile, inhibition of GX_P2V infection increased with the duration of CAP treatment (Fig. 2B). Although CAP only partially inactivated GX_P2V in response to 10 s of exposure, the decrease in infectious virions was over 90% after exposure to CAP for 60 s or more. The inhibition rate increased to 98.04% after 180 s plasma treatment and further increased to 99.94% after 300 s plasma exposure. These results indicated that GX_P2V infection was effectively inhibited by CAP treatment. Plaque forming assay results revealed little production of infectious viruses remined after CAP treatment for 180 s, with no obvious plaque observed after 10-fold dilution (Fig. 2C). Many transparent plaques were visible after $10^4$-fold dilution in the sample treated with CAP for 10 s (Fig. 2D), whereas several plaques were observed after $10^5$-fold dilution in the untreated virus sample, as indicated by the red arrow (Fig. 2E). Microscopic images further confirmed that the viral cytopathic effects of cells were reduced with increasing plasma treatment time (Fig. S2(A)). Meanwhile, the viral suspension containing phenol red turned from red to yellowish as the duration of CAP exposure increased, indicating that acidic conditions were achieved after CAP treatment (Fig. S2(B)).

### 3.2. Disinfection of pseudotyped SARS-CoV-2 variants

Six types of pseudoviruses incorporated with the S protein of SARS-CoV-2 variants were prepared and used to investigate the disinfection abilities of CAP. Vero E6 cells were used as recipients, and infection was used to evaluate the inactivation effect of CAP on S protein variants. In this study, 100 μL pseudotyped wild type and variants referred to as B.1.351 (Beta), P.1 (Gamma), B.1.526 (Lota), B.1.1.7 (Alpha), B.1.617.2 (Delta) and C.37 (lambda) were subjected to CAP for 300 s. After infection, the relative light unit (RLU) of wild type, B.1.351, B.1.526 and B.1.1.7 were decreased from $1.86 \times 10^3$, $2.14 \times 10^3$, $6.57 \times 10^3$, $6.85 \times 10^3$ and $5.37 \times 10^3$ to 15.75, 12.25, 17.25, 14.25 and,15.50 with inhibitions calculated as 99.51%, 99.74%, 99.85%, 99.90% and 99.84%, respectively; the RLU of P.1 and B.1.617.2 were decreased from $1.06 \times 10^4$ and $1.21 \times 10^4$ to 21.8 and 21.0, with inhibitions calculated as 99.84% and 99.88%, respectively (Fig. 3). Based on these results, it appeared that CAP treatment inactivated SARS-CoV-2 wild type and variant pseudoviruses by inactivating the S protein anchored in the membrane of the pseudovirions.

### 3.3. Disinfection of coronavirus SADS-CoV and PEDV

Coronavirus SADS-CoV and PEDV were also subjected to CAP exposure to investigate its inactivation ability and efficacy against coronavirus. SADS-CoV, reported by Peng et al. for the first time in 2018, is a bat-related alphacoronavirus that had led to large-scale outbreaks of fatal disease in pigs in both China and America (Zhou et al., 2018). PEDV is another alphacoronavirus that is also pathogenic to pigs (Wang et al., 2016a, 2016b), notably similar results were observed for SADS-CoV and PEDV. The inactivation efficacy of CAP increased when the viral volume decreased. When the viral volume was less than 100 μL, the reductions in both SADS-CoV and PEDV after CAP treatment for 300 s were greater than 99.74% and 99.86%, respectively (Fig. 4A and C). Similarly, the inactivation efficacy of CAP treatment increased when the duration of CAP exposure was increased. Compared to SADS-CoV, PEDV exhibited

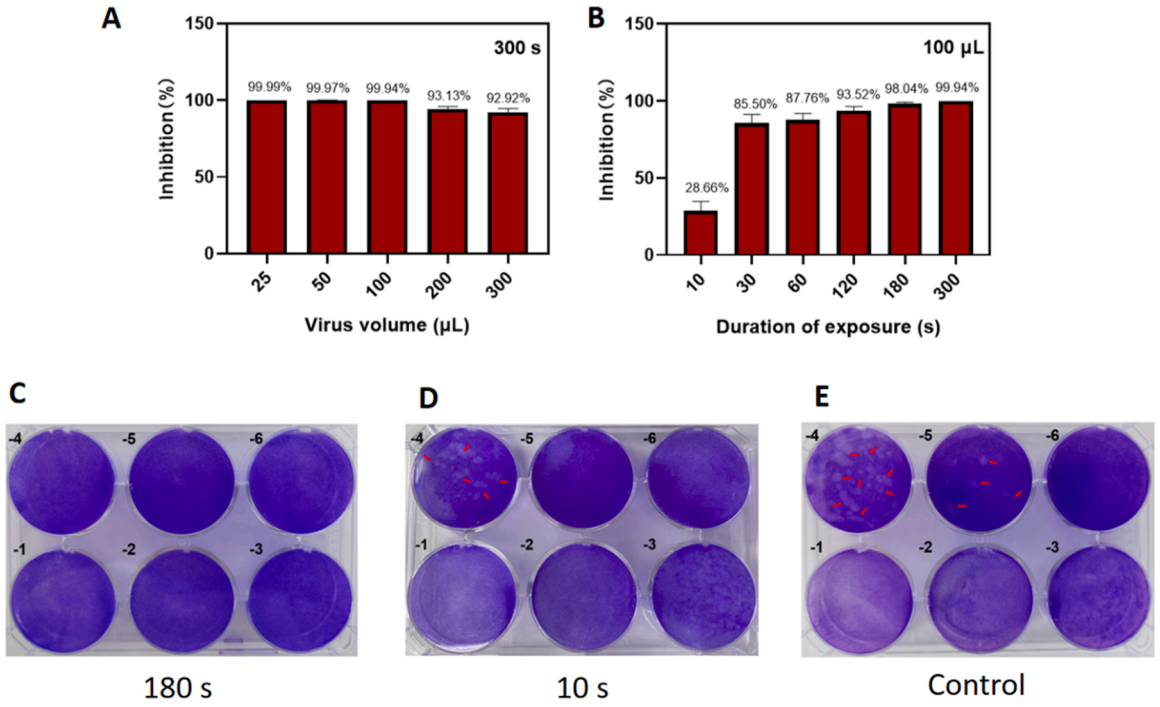


**Fig. 2.** Effects of plasma on the elimination of SARS-CoV-2-like coronavirus GX_P2V. (A) Inhibition (%) of GX_P2V at various volumes by Ar-fed CAP. The calculation of inhibition was based on the titer of the corresponding volume of GX_P2V with Ar treatment. (B) Inhibition (%) of GX_P2V at various Ar-fed CAP exposure durations. (C) Plaques produced by GX_P2V after CAP treatment for 180 s (D) Plaques produced by GX_P2V after CAP treatment for 10 s **(E)** Plaques produced by GX_P2V without CAP treated.

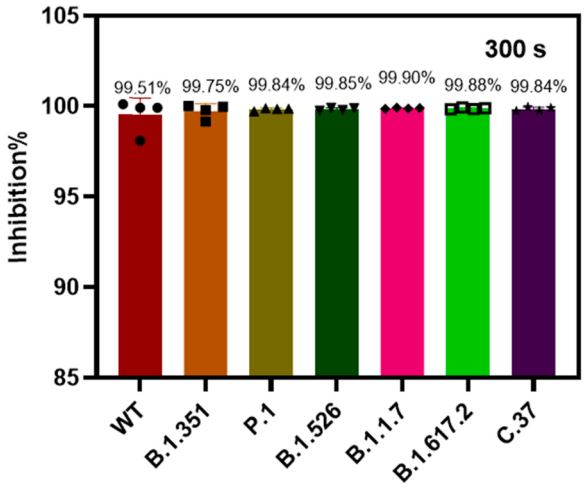


**Fig. 3.** Effect of plasma on SARS-CoV-2 wild type and variants. Pseudotyped SARS-CoV-2 wild type and five strains of variants, B.1.351 (Beta), P.1 (Gamma), B.1.526 (Lota), B.1.1.7 (Alpha), B.1.617.2 (Delta) and C.37 (lambda), were subjected to the plasma jet.

increased susceptibility to CAP treatment, with infectious virion production decreasing by 97.39% after treatment with CAP for 60 s, while the yield of infectious SADS-CoV decreased by 87.44% (Fig. 4B and D). Microscopic images of cells and color changes of the virus suspension further confirmed the disinfection effect of CAP treatment (Fig. S3 and S4). These results indicate that CAP is a promising disinfection agent for coronavirus PEDV and SADS-CoV.

### 3.4. The effect of CAP on GX_P2V particle morphology

To visually observe the mechanism of CAP exposure on virus, TEM was used to examine the morphological changes of GX_P2V particles before and after CAP treatment. Untreated GX_P2V exhibited a spherical and symmetrical morphology with an intact structure and a diameter of 100 nm (Fig. 5A). In response to CAP treatment for 180 s, distinct morphological changes were observed, with most of the particles exhibiting shrunken and irregular spherical structures (Fig. 5B). This result indicates that CAP destroyed the structure of the GX_P2V outer membrane, in which the S protein was anchored.

### 3.5. The effect of CAP on RBD at the cellular and molecular levels

Our early results indicated that CAP treatment inactivated SARS-

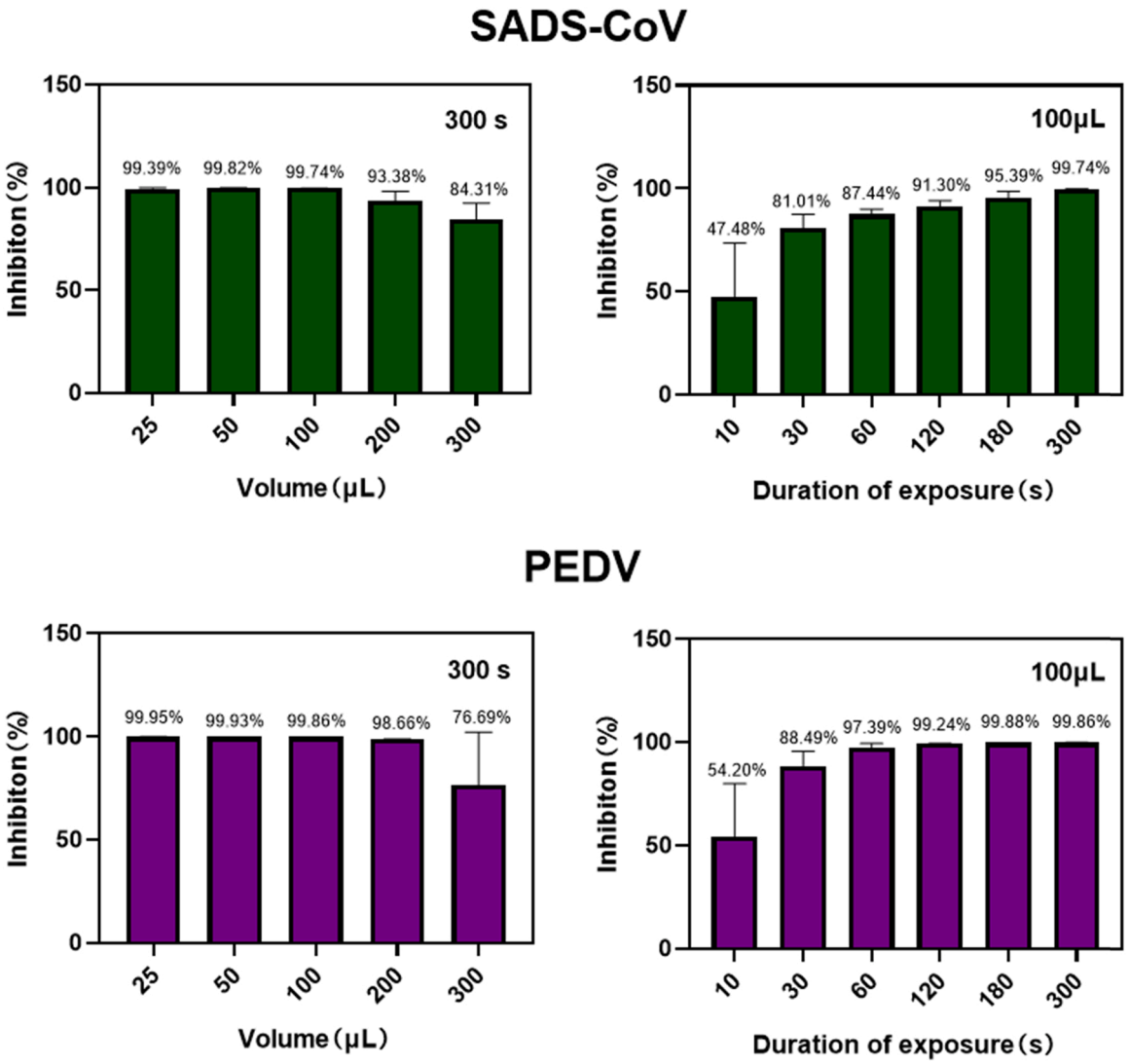


**Fig. 4. Disinfection effect of Ar-fed CAP on coronavirus SADS-CoV and PEDV. (A, C)** Inhibition (%) of SADS-CoV and PEDV at various volumes by Ar-fed CAP. **(B, D)** Inhibition (%) of SADS-CoV and PEDV at various Ar-fed CAP exposure durations.

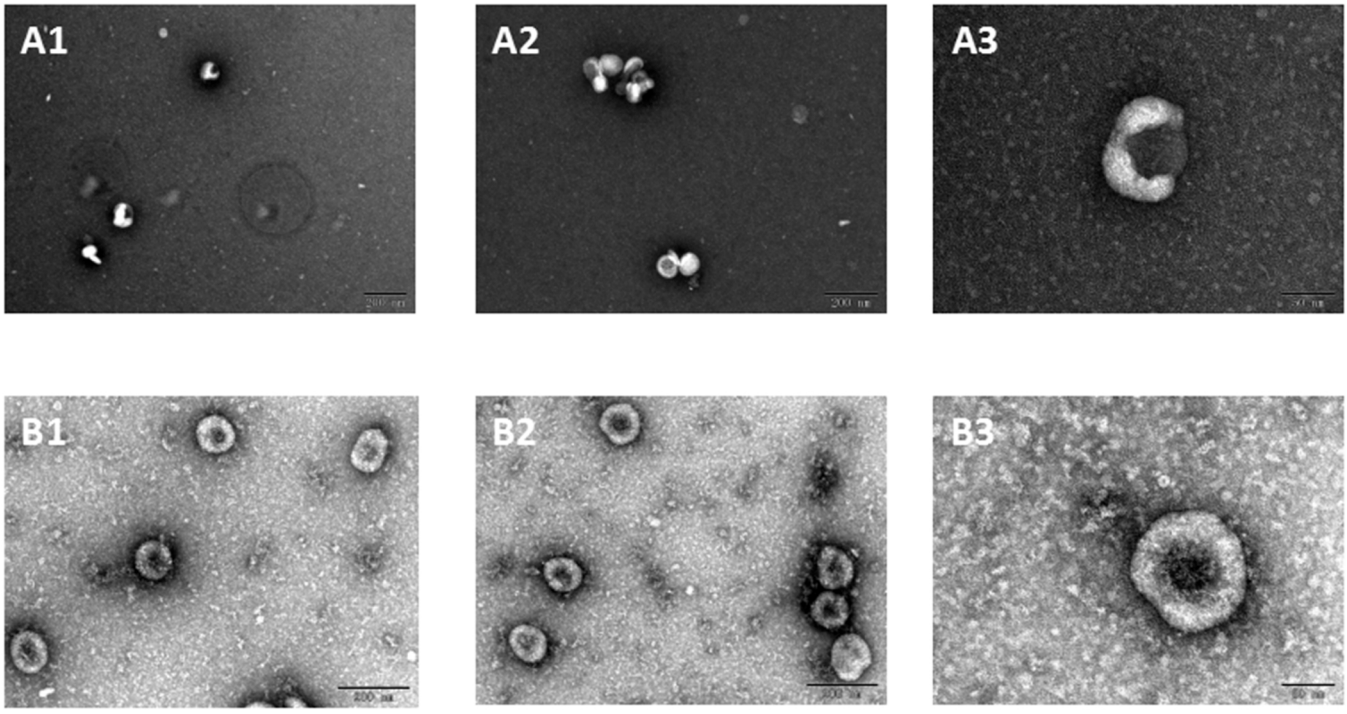


**Fig. 5.** GX_P2V images captured by TEM. (A) Transmission electron microscopy (TEM) images of GX_P2V after CAP exposure for 3 min (B) TEM images of GX_P2V not treated with CAP. The bars in A1, A2, B1 and B2 represent 200 nm.The bars in A3 and B3 represent 50 nm.

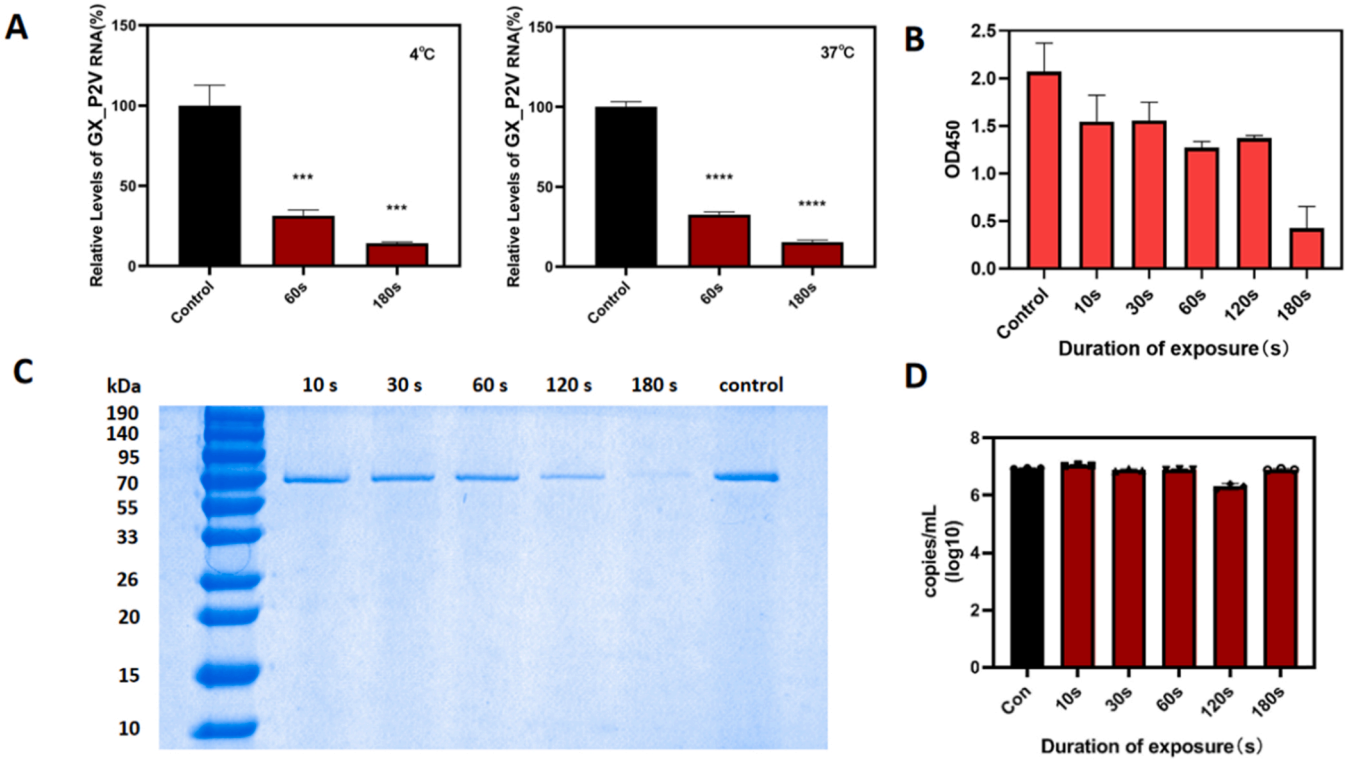


**Fig. 6.** CAP effectively inhibit GX_P2V adsorption and entry into cells and reduce the binding ability of SARS-CoV-2 RBD to hACE2, rather than degrading viral RNA. (A) The viral inactivation ability of CAP was analyzed by viral attachment assay. The virus with Ar-fed CAP treated at 60 s and 180 s was added to Vero E6 cells for attachment at 4 ℃ and for entrey at 37 ℃. The same volume of GX_P2V with only Ar treatment was used as a control. ***$p < 0.001$,****$p < 0.0001$. (B) Binding activities of the SARS-CoV-2 RBD treated with Ar-fed CAP for different durations were analyzed by ELISA. (C) SDS-PAGE analysis of RBDs with CAP-treated and untreated. (D) Viral copy number was detected by RT-qPCR. Specific primers for the S protein were employed for cDNA amplification in RT-qPCR analysis.

CoV-2 wild type and variant pseudoviruses through its inactivation of viral S protein, a structural protein that recognizes and attaches to cellular receptors (ACE2). To preliminarily verify this hypothesis, 100 μL of GX_P2V with Ar-CAP treatment for 60 s or 180 s was incubated with Vero E6 cells at 4 ℃ (for viral attachment only) and 37 ℃ (for both viral attachment and internalization) to detect attachment between the virus and cells. Treatment with CAP for 60 s and 180 s significantly reduced the relative levels of GX_P2V RNA by more than 70% ($P < 0.001$) and 85% ($P < 0.0003$), respectively (Fig. 6A), indicating that the amount of GX_P2V attached to target cells decreased in response to CAP treatment.

Next, ELISA was performed to directly examine the effect of CAP on the interaction between the SARS-CoV-2 RBD and receptor hACE2. The binding activity to hACE2 was slightly weakened when the SARS-CoV-2 RBD was exposed to CAP for 10 s ~ 120 s (Fig. 6B). When treated with CAP for 180 s, the binding activity of the SARS-CoV-2 RBD was dramatically lost. Several amino acids located in the S protein, including cysteine, tryptophan, tyrosine, histidine and methionine, become fragile when exposed to CAP. These proteins were easily oxidized by RONS generated from CAP exposure. The front view and top view of the S protein and the distribution of amino acids are shown in Fig. S5A and S5B. The structure file of the SARS-CoV-2 S protein was obtained from NCBI (PDB ID: 6VXX) (Walls et al., 2020). SDS–PAGE analysis showed that the bands of the SARS-CoV-2 RBD became obscure as the CAP treatment duration increased, suggesting that the RBD was degraded by CAP treatment (Fig. 6C). Based on the above results, it was suggested that reactive species generated in CAP caused the denaturation and even degradation of RBD, preventing its binding to cellular ACE2.

### 3.6. The effect of CAP on viral genomic RNA

To investigate the degradation of GX_P2V genomic RNA in response to CAP treatment, relative quantification of viral RNA was performed. After genomic RNA extraction, the viral RNA was reverse transcribed to cDNA for subsequent RT–qPCR analysis. No obvious difference of the spike gene amplification by Ar-fed CAP treatment was observed, even after 180 s of exposure, indicating that CAP exposure of GX_P2V had little influence on viral genomic RNA within 180 s (Fig. 6D).

### 3.7. Reactive species measurement and scavenger addition assay

It is well recognized that RONS generated by CAP is the primary feature that contributes to virus inactivation (Filipić et al., 2020). Due to their short lifespan, the measurement and identification of RONS is a challenging task (Filipić et al., 2020). Gaseous reactive species, including·OH and $N_2$ second positive system($C_3\Pi_u - B_3\Pi_g$), were detected using optical emission spectroscopy (Fig. S6). The concentrations of aqueous reactive species that ultimately function in viral disinfection

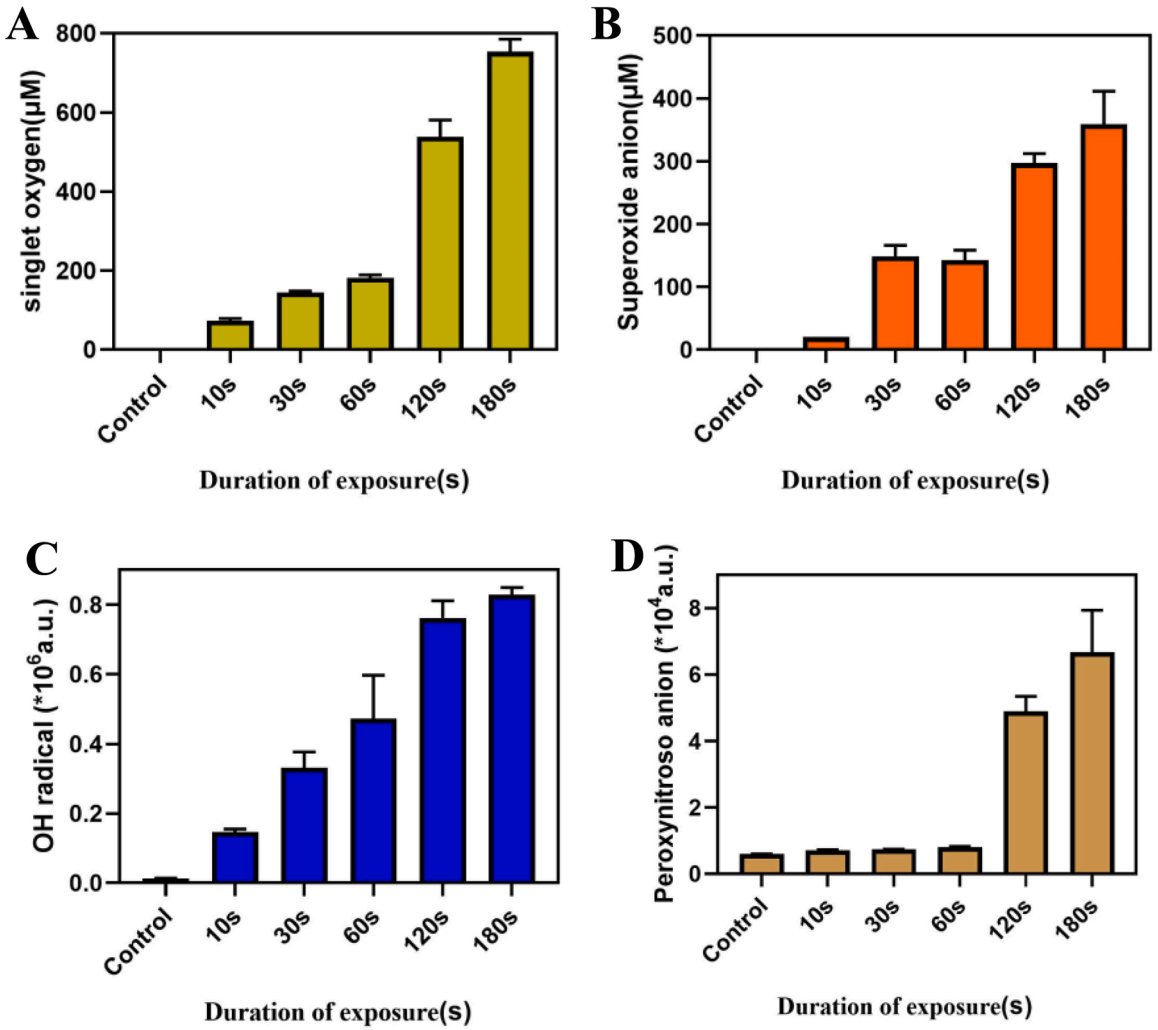


**Fig. 7.** Detection of active substances produced by plasma. (A) $^1O_2$ content produced by plasma jet in different duration of exposure. (B) $O_2^-$ content produced by plasma jet in different duration of exposure. (C) Trend of·OH content produced by plasma jet in different duration of exposure. (D) Trend of $ONOO^-$ content produced by CAP plasma jet in different duration of exposure.

efficiency were determined by the chemical reactions between gaseous RONS and water molecules (Yo et al., 2019). Due to the limitations of detection probes for short lifespan species, only a few aqueous species, including $^1O_2$, $O_2^-$,·OH and $ONOO^-$, were detected. The concentrations of these four species increased with CAP treatment time (Fig. 7A-D). In response to CAP treatment for 180 s, the concentrations of $^1O_2$ and $O_2^-$ were 753 μM and 359 μM (Fig. 7A and B), respectively. Only qualitative results were obtained for·OH and $ONOO^-$ due to the limitations of the detection kit (Fig. 7C and D). $^1O_2$ in the solution was derived from electron collision and oxygen recombination reactions (1–2) (Takamatsu et al., 2014).

$$O_2 + e \rightarrow {}^1O_2 \quad (1)$$

$$2O \rightarrow {}^1O_2 \quad (2)$$

The·OH was mainly produced through electron driven dissociation of water, and partly originated from the photolysis of water and charge exchange of incident positive ions on the gas-liquid surface via reaction (3–5) (Delgado et al., 2018; Gorbanev et al., 2016; Kristian et al., 2020).·OH was mainly produced in the region between the jet nozzle and the liquid interface and then diffused into the solution. As the relative amounts of·OH and $^1O_2$ formed in the gas depend strongly on the humidity of the feed gas, the humidity in this experiments were monitored and controlled at 65% during the experiments.

$$H_2O + e^- \rightarrow H + OH + e^- \quad (3)$$

$$HV + H_2O_{aq} \rightarrow H_{aq} + OH_{aq} \quad (4)$$

$$2H_2O_{aq} + M^+ \rightarrow M + H_3O^+_{aq} + OH_{aq} \quad (5)$$

The primary formation modes of $O_2^-$ were electron attachment formed by dissolved oxygen reactions (6) (Chen et al., 2014). Other pathways may exist through $H_2O_2$ decomposition reactions (7–9) (Liu et al., 2016).

$$O_2 + e \rightarrow O_2^- \quad (6)$$

$$H_2O_2 + NO_3 \rightarrow HO_2 + NO_3^- + H^+ \quad (7)$$

$$OH + O_3 \rightarrow HO_2 + O_2 \quad (8)$$

$$HO_2 \rightarrow O_2^- + H^+ \quad (9)$$

The formation of $ONOO^-$ primarily depends on the reaction of $NO_2$ and·OH to form ONOOH, followed by the decomposition of ONOOH to form $ONOO^-$ reactions (10–11) (Liu et al., 2016). In addition, the chemical reaction rate between $O_2^-$ and NO is extremely high ($k = 1.6 \pm 0.3 \times 10^{10}\, m^{-1}s^{-1}$) (Kissner et al., 2003). The fast increase in $ONOO^-$ concentration after 60 s of CAP treatment indicated that the reaction (12) dominated during CAP treatment between 60 s and 120 s

$$NO_2 + OH \rightarrow ONOOH \quad (10)$$

$$ONOOH \rightarrow ONOO^- + H^+ \quad (11)$$

$$NO + O_2^- \rightarrow ONOO^- \quad (12)$$

To determine the roles of short-lived active species generated by CAP in viral disinfection and RBD inactivation, scavengers of typical RONS were added in the solution. The choice of scavengers for different reactive species, including $ONOO^-$, $O_2^-$, $^1O_2$ and·OH, were supported by several literatures (Tarabová et al., 2019; Wu et al., 2012; Xu et al., 2021). The scavengers of $ONOO^-$, $O_2^-$, $^1O_2$ and·OH which were ebselen (1 mM), superoxide dismutase (SOD) (100 U/mL), L-histidine (0.05 M) and D-mannitol (0.1 M), respectively, were premixed with GX_P2V and RBD before CAP exposure. The addition of scavengers had no influence on cell survival. However, the existence of scavengers did significantly offset the disinfection effect of CAP on GX_P2V (Fig. 8A). The inactivation effect of CAP was mostly eliminated by ebselen, with infectious virion production increasing by 3.13 orders of magnitude, indicating that $ONOO^-$ plays a primary role in the CAP disinfection effect. The addition of SOD and L-histidine secondarily offset the inactivating effect of CAP by 2.85 and 2.20 orders of magnitude, respectively. The addition of D-mannitol increased the infectious virus yield by only 1.05 orders of magnitude, indicating that·OH exhibited the least disinfection effect compared to the other three short-lived active species. Furthermore, ELISA was performed to distinguish the effects of·OH, $^1O_2$, $O_2^-$ and $ONOO^-$ on the SARS-CoV-2 RBD. Similarly, the inactivation effect of CAP on the RBD was crippled by the removal of·OH, $^1O_2$, $O_2^-$ and $ONOO^-$ (Fig. 8B). Likewise, these results indicated that the quenching of $ONOO^-$ mostly eliminated the inactivation effect of CAP on the RBD. The effect of short-lived species on viral disinfection followed the order of $ONOO^- > O_2^- > {}^1O_2 >$ ·OH.

## 4. Discussion

In summary, we presented a high-performance pulse power excited CAP for the rapid disinfection of SARS-CoV-2-like coronaviruses GX_P2V, pseudotyped SARS-CoV-2 and other coronaviruses. The infectious GX_P2V production measured by the TCID50 assay decreased by 99.94% after 300 s of CAP exposure, indicating that CAP-treated viruses exhibited nearly abolished infectivity. The inhibition rate of SARS-CoV-2 pseudotyped variants was greater than 99.50% after 300 s of CAP treatment. As expected, CAP treatment also exhibited excellent inhibition of swine coronavirus SADS-CoV and PEDV, with inhibiton rates of 99.74% and 99.86%. These results are comparable with widely employed disinfectants such as $H_2O_2$, $O_3$, peracetic acid, or UV. Criscuolo et al. investigated the inactivation efficacies of SARS-CoV-2 by ultraviolet light (UV) and ozone ($O_3$), and infectious SARS-CoV-2 particles reduced by $>$ 99.9% after UV irradiation at a work distance of 20 cm for 15 min in a well plate, and by $>$ 90% after 4 ppm $O_3$ for 30 min on six common materials. Chemical disinfectant involving peracetic acid, hydrogen peroxide exhibit rapid virucidal ability in 5 min ( $\approx$ 4 log10 reduction) and 1 min ( $>$ 4 log10 reduction), respectively (Becker et al., 2017; Criscuolo et al., 2021; Omidbakhsh and Sattar, 2006). Indeed, each of the developed methods have their own strengths and shortcomings, and the virucidal efficacies of above disinfection approaches were somehow obtained from the labs. The presence of natural interfering substances (e.g. saliva, mucus etc) under real-world conditions are highly likely to significantly reduce the effectiveness of the disinfection approach and warrant further studies (Chen et al., 2020; Šimončicová et al., 2019). Although CAP showed great potential for virus disinfection, the small treatment area of a single plasma jet makes it difficult for large-scale industrial applications. Large treatment areas might be achieved by grouping many individual plasma jet together, which provided an industrial application possibility (Wang et al., 2017).

The pulsed excited CAP employed in this work provided high instantaneous power and plasma activity, which was responsible for the rapid disinfection rate (Fig. S1A). The amplitudes of the applied voltage and plasma current of the pulsed excited CAP were 8.5 kV and 2 A, respectively (Fig. S1B). Due to the short duration of pulse-on time, the average power was quite low (10.89 W), making it a power-saving technology. In addition, the effect of temperature was considered. The pulse-powered CAP exhibited a slight temperature increase (~34 ℃) compared to traditional AC-powered CAP (54 ℃) after 180 s of treatment (Fig. S7A and S7B). The coronaviruses in solution retained viability for 1~2 days at a temperature range of 33–37 ℃ (Chan et al., 2020). Thus, the temperature factor can be excluded due to the short CAP treatment time used for these tests. RONS with high oxidation ability were believed to be the primary factors for CAP-mediated-viral disinfection (Fig. 9).

Proteins are major biological targets for radicals due to their high rate constants for reaction (Min et al., 2014). Although there are studies reported on different extent of viral RNA damage occurring during

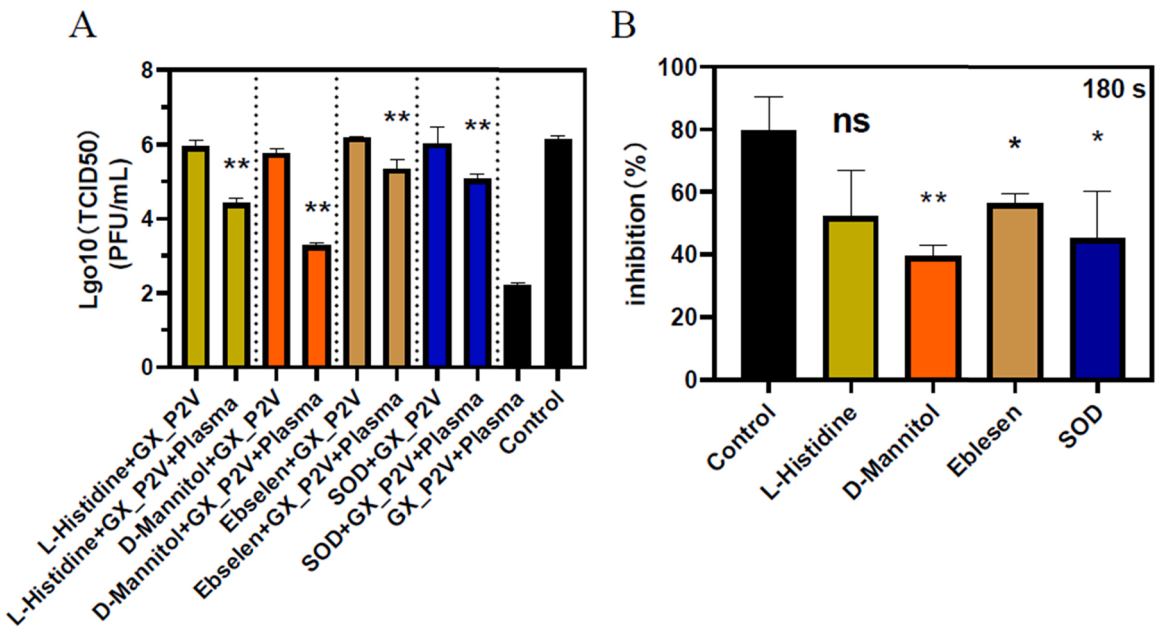


**Fig. 8.** Functional examination of short-lived reactive species by adding quenchers to the GX_P2V and SARS-CoV-2 RBDs. (A) The titers of GX_P2V premixed with quencher after 180 s of treatment with CAP were measured using TCID50 assay. * *p < 0.01. (B) Analysis of binding between RBD premixed with quencher and hACE2 after 180 s of CAP treatment by ELISA. *p < 0.05, **p < 0.01.

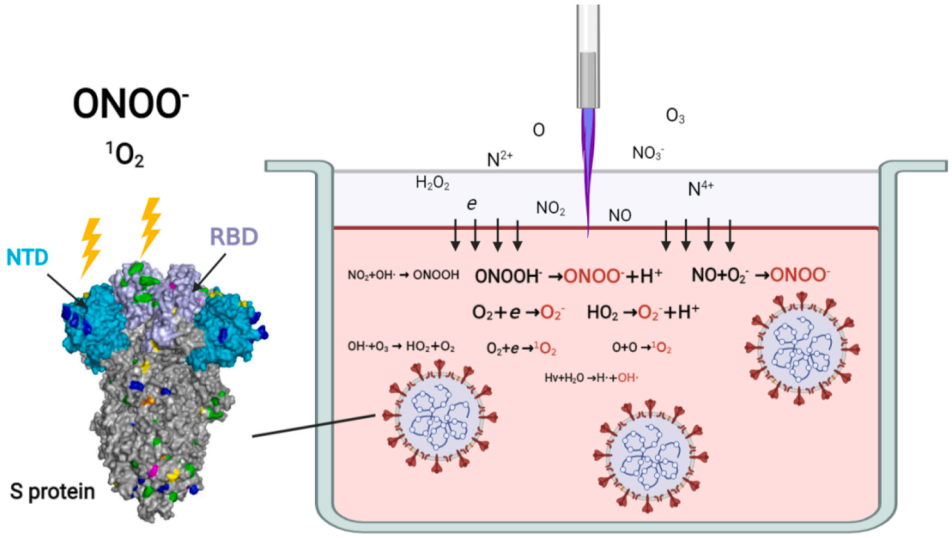


**Fig. 9.** Mechanism of RONS generated in Ar-fed CAP damaging S protein. Reactive species generated by plasma jet disslove into liquid and cross-react in liquid phase. Predominant RONS $ONOO^-$ and $O_2^-$ caused oxidation to tyrosine, tryptophan and histidine that located at RBD and NTD, which may impair the binding ability of RBD to cell receptor ACE2 and the function of NTD. The viral genome remained intact after 3 min-CAP treatment.

plasma treatment, we did not observed significant discrepancy presented in the levels of intact RNA by PCR amplification in 3 min-treatment (Fig. 6D) (Aboubakr et al., 2018; Yamashiro et al., 2018). Due to the nonspecific reaction of CAP-induced reactive species, all outer proteins of the virus inevitably react with CAP, which may affect binding to target cells and viral morphology, ultimately impairing infection ability. The addition of ebselen, a scavenger for $ONOO^-$, largely suppressed the reduction of GX_P2V infection and SARS-CoV-2 RBD binding activity (Fig. 8A and B), which indicated that $ONOO^-$ plays a primary role in virus disinfection by our Ar-fed CAP. It is speculated that $ONOO^-$ is the primary reactive substance of the CAP-treated liquid, which is directly generated by the plasma jet and transformed from $O_2^-$, $NO^-$, $NO_2^-$ and $H_2O_2$ (Eqs. 7and 9). The addition of L-histidine and SOD resulted in slightly less pronounced reduction effects of disinfection and inactivation, indicating that $^1O_2$ and $O_2^-$ play secondary roles. The elimination of·OH only suppressed the disinfection effect by 1.05 orders of magnitude and showed the least neutralization of RBD inactivation, suggesting that·OH does not play a key role in our Ar-fed CAP. This observation may be explained by a pathway in which·OH changes into dissolved $O_2$ and reacts with electrons to yield $O_2^-$. Our results are basically in agreement with those of Gracanin M. et al. and Aboubakr, H et al., who proposed that $^1O_2$ is a dominant species generated by CAP and is responsible for virus disinfection but that·OH does not play a key role (Aboubakr et al., 2016; Akan and Çabuk, 2014; Gracanin et al., 2009). The exact composition that CAP generated depends on the component of the gas ignitor, and the role that reactive species may play varies based on different gas conditions(Akan and Çabuk, 2014; Filipić et al., 2021).

The distribution of four typical amino acids, cysteine, tryptophan, tyrosine and methionine, in the SARS-CoV-2 S protein and RBD was indicated in the conformational landscape of the SARS-CoV-2 trimeric S protein to better study the inactivating effect of CAP on S proteins (Fig. S5). Tyrosine exhibited a tendency to be oxidized due to the hydroxy-substitution of the phenolic ring. Histidine and tryptophan possess a C═C bond, while cysteine and methionine contain a sulfur atom, making them susceptible to oxidation. Tyrosine is susceptible to $^1O_2$, $O_2^-$ and $ONOO^-$, resulting in oxidative modification (Davies, 2016; Gracanin et al., 2009; Radi, 2013). It is the most abundant amino acid in the GX_P2V S protein and SARS-CoV-2 RBD, accounting for 4.41% and 6.88%, respectively. Tyrosine has no direct reaction with $ONOO^-$, whose oxidation and nitration are accomplished by peroxynitrite-derived radicals, resulting in the production of 3-nitrotyrosine and 3-hydroxytyrosine (Alvarez and Radi, 2003; Radi, 2013). The reaction of tyrosine and $^1O_2$ leads to ring-derived hydroperoxides (Gracanin et al., 2009). Chi et al. revealed that NTD-targeting antibody prevents infection of both authentic and pseudotyped SARS-CoV-2 in vitro, suggesting that dysfunction of the S protein NTD led to the disinfection of SARS-CoV-2 (Chi et al., 2020). Histidine is thought to be one of the major targets for $^1O_2$ attack (Kim et al., 2008). $^1O_2$-mediated oxidation of histidine results in a mixture of products via the 1,4-cycloaddition of $^1O_2$ to the imidazole ring, resulting in the formation of one or more endoperoxides (Gracanin et al., 2009). Cysteine and methionine are thought to react with $ONOO^-$ and $^1O_2$ with rate constants on the order of $10^2 \sim 10^3\ m^{-1}\ s^1$. Overall, the RONS produced by CAP - induced oxidative damage to the viral S protein at specific residues rather than causing damage to genomic RNA (no damage to viral RNA during plasma processing (Fig. 6D)), crippling the binding ability of the S protein to cellular receptors and preventing infection of cells.

## 5. Conclusions

In conclusion, Ar-fed CAP effectively inactivated SARS-CoV-2-like coronavirus GX_P2V and SARS-CoV-2 pseudotyped virus for both wild type and variants within 180 s. The potent inactivation ability of CAP was also reflected in swine coronavirus PEDV and SADS-CoV. Morphological analysis, pseudovirus assays and RBD binding tests demonstrated that virus-binding proteins are subjected to reactive species, such as RONS generated by CAP, leading to morphological changes and loss of infectivity. The effect of RONS followed the order of $ONOO^- > O_2^- > {}^1O_2 > \cdot OH$. CAP treatment does not cause secondary pollution or an increase in temperature, exhibiting great potential to eliminate the coronavirus as a novel form of surface sterilization.

## Novelty Statement

Here, we introduce and evaluate a novel surface disinfection strategy to coronavirus. Our results found that cold atmospheric pressure plasma (CAP) disinfects coronavirus particles in 5 min and does negligible harm to environment and human, which advantages over other surface disinfections. In this work we firstly describe the broad-spectrum disinfection of CAP on coronaviruses. We firstly access the disinfection effect of CAP on SARS-CoV-2 and its dominant variants, and explore the oxidative effect based on the amino acid sequence and structure of S protein.

## Author Contributions

R.-X. W., H.-H. F. and Y.-G. T. developed the concept. R.-X. W., H.-H. F., H.-B. Q., H.-J. Q. and S.-T. H. designed the research scheme. H.-B. Q. and S.-T. H. performed the virus and protein inactivation test. H.-J. Q. performed the plasma characterization and radical measurement assay. B.-X. H., K. L, F.-X. L. and M.-C. L.prepared the pseudovirus and performed the relevant tests. K. L., M.-F. P and P.-J. H prepared the viruses. H.-B. Q, H.-J. Q. and S.-T. H. analyzed the data. R.-X. W., H.-J. Q., P. H., X.-H. K. and Y.-J. S established the plasma generator. S.-T. H., H.-J. Q and H.-B. Q drafted the manuscript. H.-H. F., R.-X. W. and Y.-G. T provided important experimental insights.

## Declaration of Competing Interest

The authors declare no competing interests.

## Data Availability

All data needed to evaluate the conclusions in the paper are present in the paper and/or the Supplementary Materials.

## Acknowledgements

None.

*Funding*

This research was supported by National Natural Science Foundation of China (NO. 51877205, 52011530191), the Fundamental Research Funds for the Central Universities (BUCTRC201906, BUCTZY2022, China), Key Project of Beijing University of Chemical Technology (No. XK1803-06, China), National Key Research and Development Program of China (NO. 2018YFA0903000, 2020YFA0712102), Funds for First-class Discipline Construction (No. XK1805, China).

## Appendix A. Supporting information

Supplementary data associated with this article can be found in the online version at doi:10.1016/j.jhazmat.2022.128414.

## References

Aboubakr, H.A., Williams, P., Gangal, U., Youssef, M.M., El-Sohaimy, S.A., Bruggeman, P.J., Goyal, S.M., 2015. Virucidal effect of cold atmospheric gaseous plasma on feline calicivirus, a surrogate for human norovirus. Appl. Environ. Microbiol. 81 (11), 3612–3622.

Aboubakr, H.A., Gangal, U., Youssef, M.M., Goyal, S.M., Bruggeman, P.J., 2016. Inactivation of virus in solution by cold atmospheric pressure plasma: identification of chemical inactivation pathways. J. Phys. D Appl. Phys. 49, 204001.

Aboubakr, H.A., Mor, S.K., Higgins, L., Armien, A., Youssef, M.M., Bruggeman, P.J., Goyal, S.M., 2018. Cold argon-oxygen plasma species oxidize and disintegrate capsid protein of feline calicivirus. PLoS One 13 (3), e0194618.

Alvarez, B., Radi, R., 2003. Peroxynitrite reactivity with amino acids and proteins. Amino Acids 25, 295–311.

Becker, B., Brill, F., Todt, D., Steinmann, E., Lenz, J., Paulmann, D., Bischoff, B., Steinmann, J., 2017. Virucidal efficacy of peracetic acid for instrument disinfection. Antimicrob. Resist. 6, 114.

Bernhardt, T., Semmler, M.L., Schäfer, M., Bekeschus, S., Emmert, S., Boeckmann, L., 2019. Plasma medicine: applications of cold atmospheric pressure plasma in dermatology. Oxid. Med. Cell. Longev. 2019, 3873928-10.

Bourke, P., Ziuzina, D., Boehm, D., Cullen, P.J., Keener, K., 2018. The potential of cold plasma for safe and sustainable food production. Trends Biotechnol. 36, 615–626.

Chan, K.H., Sridhar, S., Zhang, R.R., Chu, H., Fung, A.Y., Chan, G., Chan, J.F., To, K.K., Hung, I.F., Cheng, V.C., Yuen, K.Y., 2020. Factors affecting stability and infectivity of SARS-CoV-2. J. Hosp. Infect.. 106, 226–231.

Chen, C., Liu, D.X., Liu, Z.C., Yang, A.J., Chen, H.L., Shama, G., Kong, M.G., 2014. A model of plasma-biofilm and plasma-tissue interactions at ambient pressure. Plasma Chem. Plasma Process. 34 (3), 403–441.

Chen, Z., Simonyan, H., Cheng, X., Gjika, E., Lin, L., Canady, J., Sherman, J.H., Young, C., Keidar, M., 2017. A novel micro cold atmospheric plasma device for glioblastoma both in vitro and in vivo. Cancers (Basel) 9 (6), 61.

Chen, Z., Garcia Jr., G., Arumugaswami, V., Wirz, R.E., 2020. Cold atmospheric plasma for SARS-CoV-2 inactivation. Phys. Fluids(1994) 32 (11), 111702.

Chi, X., Yan, R., Zhang, J., Zhang, G., Zhang, Y., Hao, M., Zhang, Z., Fan, P., Dong, Y., Yang, Y., Chen, Z., Guo, Y., Zhang, J., Li, Y., Song, X., Chen, Y., Xia, L., Fu, L., Hou, L., Xu, J., Yu, C., Li, J., Zhou, Q., Chen, W., 2020. A neutralizing human antibody binds to the N-terminal domain of the Spike protein of SARS-CoV-2. Science 369, 650–655.

Cote, Chelsea, Schneider, D., Stephanie, R., Lyu, Ming, Gao, Sherry, 2018. Photochemical production of singlet oxygen by urban road dust. Environ. Sci. Technol. Lett. 5, 92–97.

Criscuolo, E., Diotti, R.A., Ferrarese, R., Alippi, C., Viscardi, G., Signorelli, C., Mancini, N., Clementi, M., Clementi, N., 2021. Fast inactivation of SARS-CoV-2 by

UV-C and ozone exposure on different materials. Emerg. Microbes Infect. 10 (1), 206–210.
Davies, M.J., 2016. Protein oxidation and peroxidation. Biochem. J. 473, 805–825.
Dehning, J., Zierenberg, J., Spitzner, F.P., Wibral, M., Neto, J.P., Wilczek, M., Priesemann, V., 2020. Inferring change points in the spread of COVID-19 reveals the effectiveness of interventions. Science 369 (6500).
Delgado, H.E., Rumbach, P., Bartels, D.M., Go, D.B., 2018. Total internal reflection absorption spectroscopy (TIRAS) for the detection of solvated electrons at a plasma-liquid interface. J. Vis. Exp.
Drayman, N., DeMarco, J.K., Jones, K.A., Azizi, S.A., Froggatt, H.M., Tan, K., Maltseva, N.I., Chen, S., Nicolaescu, V., Dvorkin, S., Furlong, K., Kathayat, R.S., Firpo, M.R., Mastrodomenico, V., Bruce, E.A., Schmidt, M.M., Jedrzejczak, R., Muñoz-Alía, M.Á., Schuster, B., Nair, V., Han, K.Y., O&#39, Brien, A., Tomatsidou, A., Meyer, B., Vignuzzi, M., Missiakas, D., Botten, J.W., Brooke, C.B., Lee, H., Baker, S.C., Mounce, B.C., Heaton, N.S., Severson, W.E., Palmer, K.E., Dickinson, B.C., Joachimiak, A., Randall, G., Tay, S., 2021. Masitinib is a broad coronavirus 3CL inhibitor that blocks replication of SARS-CoV-2. Science 373, 931–936.
Fan, H., Hong, B., Luo, Y., Peng, Q., Wang, L., Jin, X., Chen, Y., Hu, Y., Shi, Y., Li, T., Zhuang, H., Zhou, Y., Tong, Y., Xiang, K., 2020a. The effect of whey protein on viral infection and replication of SARS-CoV-2 and pangolin coronavirus *in vitro*. Signal Transduct Target Ther . 5 (1), 275.
Fan, H., Lou, F., Fan, J., Li, M., Tong, Y., 2022. The emergence of powerful oral anti-COVID-19 drugs in the post-vaccine era. Lancet Microbe. 2, e91.
Filipić, A., Gutierrez-Aguirre, I., Primc, G., Mozetič, M., Dobnik, D., 2020. Cold plasma, a new hope in the field of virus inactivation. Trends Biotechnol. 38, 1278–1291.
Fan, H.H., Wang, L.Q., Liu, W.L., An, X.P., Liu, Z.D., He, X.Q., Song, L.H., Tong, Y.G., 2020b. Repurposing of clinically approved drugs for treatment of coronavirus disease 2019 in a 2019-novel coronavirus-related coronavirus model. Chin. Med. J. 133 (9), 1051–1056.
Filipić, A., Dobnik, D., Tušek Žnidarič, M., Žegura, B., Štern, A., Primc, G., Mozetič, M., Ravnikar, M., Žel, J., Gutierrez Aguirre, I., 2021. Inactivation of pepper mild mottle virus in water by cold atmospheric plasma. Front. Microbiol. 12, 618209.
Gorbanev, Y., O&#39, Connell, D., Chechik, V., 2016. Non-thermal plasma in contact with water: the origin of species. Chemistry 22, 3496–3505.
Gracanin, M., Hawkins, C.L., Pattison, D.I., Davies, M.J., 2009. Singlet-oxygen-mediated amino acid and protein oxidation: formation of tryptophan peroxides and decomposition products. Free Radic. Biol. Med. 47, 92–102.
Guo, L., Xu, R., Gou, L., Liu, Z., Zhao, Y., Liu, D., Zhang, L., Chen, H., Kong, M.G., 2018. Mechanism of virus inactivation by cold atmospheric-pressure plasma and plasma-activated water. Appl. Environ. Microbiol 84 (17).
Guo, L., Yao, Z., Yang, L., Zhang, H., Qi, Y., Gou, L., Xi, W., Liu, D., Zhang, L., Cheng, Y., Wang, X., Rong, M., Chen, H., Kong, M.G., 2021. Plasma-activated water: an alternative disinfectant for S protein inactivation to prevent SARS-CoV-2 infection. Chem. Eng. J. 421, 127742.
Heilingloh, C.S., Aufderhorst, U.W., Schipper, L., Dittmer, U., Witzke, O., Yang, D., Zheng, X., Sutter, K., Trilling, M., Alt, M., Steinmann, E., Krawczyk, A., 2020. Susceptibility of SARS-CoV-2 to UV irradiation. Am. J. Infect. Control 48 (10), 1273–1275.
Hijnen, W.A., Beerendonk, E.F., Medema, G.J., 2006. Inactivation credit of UV radiation for viruses, bacteria and protozoan (oo)cysts in water: a review. Water Res. 40 (1), 3–22.
Hu, Y., Liu, M., Qin, H., Lin, H., An, X., Shi, Z., Song, L., Yang, X., Fan, H., Tong, Y., 2021. Artemether, Artesunate, Arteannuin B, Echinatin, Licochalcone B and Andrographolide Effectively Inhibit SARS-CoV-2 and Related Viruses *In Vitro*. Front Cell Infect Microbiol. 11, 680127.
Kampf, G., Todt, D., Pfaender, S., Steinmann, E., 2020. Persistence of coronaviruses on inanimate surfaces and their inactivation with biocidal agents. J. Hosp. Infect. 104 (3), 246–251.
Kanazawa, S., Kawano, H., Watanabe, S., Furuki, T., Akamine, S., Ichiki, R., Ohkubo, T., Kocik, M., Mizeraczyk, J., 2011. Observation of OH radicals produced by pulsed discharges on the surface of a liquid. Plasma Sources Sci. Trans. 20, 20.
Keudell, Av, Awakowicz, P., Benedikt, J., Raballand, V., Yanguas-Gil, A., Opretzka, J., Flötgen, C., Reuter, R., Byelykh, L., Halfmann, H., Stapelmann, K., Denis, B., Wunderlich, J., Muranyi, P., Rossi, F., Kylián, O., Hasiwa, N., Ruiz, A., Rauscher, H., Sirghi, L., Comoy, E., Dehen, C., Challier, L., Deslys, J.P., 2010. Inactivation of bacteria and biomolecules by low-pressure plasma discharges. Plasma Process Polym. 7 (3–4), 327–352.
Kim, J., Rodriguez, M.E., Guo, M., Kenney, M.E., Oleinick, N.L., Anderson, V.E., 2008. Oxidative modification of cytochrome c by singlet oxygen. Free Radic. Biol. Med. 44, 1700–1711.
Kissner, R., Nauser, T., Kurz, C., Koppenol, W.H., 2003. Peroxynitrous acid–where is the hydroxyl radical. Iubmb Life 55, 567–572.
Kristian, W., Giuliana, B., Michael, L., Klaus-Dieter, W., Woedtke, T., Sander, B., Jan-Wilm, L., 2020. On a heavy path – determining cold plasma-derived short-lived species chemistry using isotopic labelling. RSC Adv. 10.
Lam, T.T., Jia, N., Zhang, Y.W., Shum, M.H., Jiang, J.F., Zhu, H.C., Tong, Y.G., Shi, Y.X., Ni, X.B., Liao, Y.S., Li, W.J., Jiang, B.G., Wei, W., Yuan, T.T., Zheng, K., Cui, X.M., Li, J., Pei, G.Q., Qiang, X., Cheung, W.Y., Li, L.F., Sun, F.F., Qin, S., Huang, J.C., Leung, G.M., Holmes, E.C., Hu, Y.L., Guan, Y., Cao, W.C., 2020. Identifying SARS-CoV-2-related coronaviruses in Malayan pangolins. Nature 583 (7815), 282–285.
Latinne, A., Hu, B., Olival, K.J., Zhu, G., Zhang, L., Li, H., Chmura, A.A., Field, H.E., Zambrana-Torrelio, C., Epstein, J.H., Li, B., Zhang, W., Wang, L.F., Shi, Z.L., Daszak, P., 2020. Origin and cross-species transmission of bat coronaviruses in China. Nat. Commun. 11 (1), 4235.
Li, M., Lou, F., Fan, H., 2021a. SARS-CoV-2 variants: a new challenge to convalescent serum and mRNA vaccine neutralization efficiency. Signal Transduct. Target. Ther. 6, 151.
Li, M., Lou, F., Fan, H., 2021b. SARS-CoV-2 Variants of Concern Delta: a great challenge to prevention and control of COVID-19. Signal Transduct Target Ther. 6 (1), 349.
Li, M., Lou, F., Fan, H., 2022. SARS-CoV-2 variant Omicron: currently the most complete "escapee" from neutralization by antibodies and vaccines. Signal Transduct Target. Ther. 7 (1), 28.
Li, S., Liu, W., Chen, Y., Wang, L., An, W., An, X., Song, L., Tong, Y., Fan, H., Lu, C., 2021b. Transcriptome analysis of cepharanthine against a SARS-CoV-2-related coronavirus. Brief. Bioinform. 22 (2), 1378–1386.
Li, W., Yu, H., Ding, D., Chen, Z., Wang, Y., Wang, S., Li, X., Keidar, M., Zhang, W., 2019. Cold atmospheric plasma and iron oxide-based magnetic nanoparticles for synergetic lung cancer therapy. Free Radic. Biol. Med. 130, 71–81.
Liu, D.X., Liu, Z.C., Chen, C., Yang, A.J., Li, D., Rong, M.Z., Chen, H.L., Kong, M.G., 2016. Aqueous reactive species induced by a surface air discharge: heterogeneous mass transfer and liquid chemistry pathways. Sci. Rep. 6, 23737.
Lou, F., Li, M., Pang, Z., Jiang, L., Guan, L., Tian, L., Hu, J., Fan, J., Fan, H., 2021. Understanding the Secret of SARS-CoV-2 Variants of Concern/Interest and Immune Escape. Front Immunol . 12, 744242.
Metelmann, H.R., Woedtke, T.V., Bussiahn, R., Weltmann, K.D., Rieck, M., Khalili, R., Podmelle, F., Waite, P.D., 2012. Experimental recovery of $CO_2$-laser skin lesions by plasma stimulation. Am. J. Cosmet. Surg. 29, 52–56.
Min, L., Zhongqi, Z., Janet, C., Da, R., Sunny, Z.Z., 2014. Discovery and characterization of a photo-oxidative histidine-histidine cross-link in IgG1 antibody utilizing 18O-labeling and mass spectrometry. Anal. Chem. 86.
Nicol McKayla, J., Brubaker Timothy, R., Honish Brian, J., Simmons Alyssa, N., Ali, K., Geissel Madison, A., Whalen Connor, T., Siedlecki Christopher, A., Bilén Sven, G., Knecht Sean, D., Kirimanjeswara Girish, S., 2020. Antibacterial effects of low-temperature plasma generated by atmospheric-pressure plasma jet are mediated by reactive oxygen species. Sci. Rep. 10 (1), 3066.
Nie, J., Li, Q., Wu, J., Zhao, C., Hao, H., Liu, H., Zhang, L., Nie, L., Qin, H., Wang, M., Lu, Q., Li, X., Sun, Q., Liu, J., Fan, C., Huang, W., Xu, M., Wang, Y., 2020. Quantification of SARS-CoV-2 neutralizing antibody by a pseudotyped virus-based assay. Nat. Protoc. 15, 3699–3715.
Noorimotlagh, Z., Mirzaee, S.A., Jaafarzadeh, N., Maleki, M., Kalvandi, G., Karami, C., 2021. A systematic review of emerging human coronavirus (SARS-CoV-2) outbreak: focus on disinfection methods, environmental survival, and control and prevention strategies. Environ. Sci. Pollut. Res. Int. 28 (1), 1–15.
Ohashi, H., Watashi, K., Saso, W., Shionoya, K., Iwanami, S., Hirokawa, T., Shirai, T., Kanaya, S., Ito, Y., Kim, K.S., Nomura, T., Suzuki, T., Nishioka, K., Ando, S., Ejima, K., Koizumi, Y., Tanaka, T., Aoki, S., Kuramochi, K., Suzuki, T., Hashiguchi, T., Maenaka, K., Matano, T., Muramatsu, M., Saijo, M., Aihara, K., Iwami, S., Takeda, M., McKeating, J.A., Wakita, T., 2021. Potential anti-COVID-19 agents, cepharanthine and nelfinavir, and their usage for combination treatment. iScience 24, 102367.
Omidbakhsh, N., Sattar, S.A., 2006. Broad-spectrum microbicidal activity, toxicologic assessment, and materials compatibility of a new generation of accelerated hydrogen peroxide-based environmental surface disinfectant. Am. J. Infect. Control 34, 251–257.
Pei, P., Qin, H., Chen, J., Wang, F., He, C., He, S., Hong, B., Liu, K., Qiao, R.Z., Fan, H., Tong, Y.G., Chen, L., Luo, S.Z., 2021. Computational design of ultrashort peptide inhibitors of the receptor-binding domain of the SARS-CoV-2 S protein. Brief. Bioinform. 22 (6).
Radi, R., 2013. Peroxynitrite, a stealthy biological oxidant. J. Biol. Chem.. 288, 26464–26472.
Sakudo, A., Yagyu, Y., Onodera, T., 2019. Disinfection and sterilization using plasma technology: fundamentals and future perspectives for biological applications. Int J. Mol. Sci. 20 (20).
Šimončicová, J., Kryštofová, S., Medvecká, V., Ďurišová, K., Kaliňáková, B., 2019. Technical applications of plasma treatments: current state and perspectives. Appl. Microbiol. Biotechnol. 103, 5117–5129.
Song, K., Wang, H., Jiao, Z., Qu, G., Chen, W., Wang, G., Wang, T., Zhang, Z., Ling, F., 2022. Inactivation efficacy and mechanism of pulsed corona discharge plasma on virus in water. J. Hazard. Mater. 422, 126906.
Takamatsu, T., Uehara, K., Sasaki, Y., Miyahara, H., Matsumura, Y., Iwasawa, A., Ito, N., Azuma, T., Kohno, M., Okino, A., 2014. Investigation of reactive species using various gas plasmas. RSC Adv. 4, 39901–39905.
Tarabová, B., Lukeš, P., Hammer, M.U., Jablonowski, H., von Woedtke, T., Reuter, S., Machala, Z., 2019. Fluorescence measurements of peroxynitrite/peroxynitrous acid in cold air plasma treated aqueous solutions. Phys. Chem. Chem. Phys.: PCCP 21, 8883–8896.
Tx, A., My, B., Im, C., Eml, D., Bo, C., Dz, C., Mt, B., Hlc, A., 2020. Inactivation of airborne porcine reproductive and respiratory syndrome virus (PRRSv) by a packed bed dielectric barrier discharge non-thermal plasma. J. Hazard. Mater. 393.
Vilcassim, M., Callahan, A.E., Zierold, K.M., 2021. Travelling to polluted cities: a systematic review on the harm of air pollution on international travellers' health. J. Travel Med. 28 (4).
Walcher, L., Kistenmacher, A.K., Sommer, C., Böhlen, S., Ziemann, C., Dehmel, S., Braun, A., Tretbar, U.S., Klöß, S., Schambach, A., Morgan, M., Löffler, D., Kämpf, C., Blumert, C., Reiche, K., Beckmann, J., König, U., Standfest, B., Thoma, M., Makert, G.R., Ulbert, S., Kossatz-Böhlert, U., Köhl, U., Dünkel, A., Fricke, S., 2021. Low energy electron irradiation is a potent alternative to gamma irradiation for the inactivation of (CAR-)NK-92 cells in ATMP manufacturing. Front. Immunol. 12, 684052.

Walls, A.C., Park, Y.J., Tortorici, M.A., Wall, A., McGuire, A.T., Veesler, D., 2020. Structure, function, and antigenicity of the SARS-CoV-2 spike glycoprotein. Cell 181, 281–292 e6.

Wang, D., Fang, L., Xiao, S., 2016a. Porcine epidemic diarrhea in China. Virus Res. 226, 226-13.

Wang, R., Gao, Y., Zhang, C., Yan, P., Shao, T., 2016b. Dynamics of plasma bullets in a microsecond-pulse-driven atmospheric-pressure he plasma jet. IEEE Trans. Plasma Sci. 44 (4), 393–397.

Wang, R., Sun, H., Zhu, W., Zhang, C., Zhang, S., Shao, T., 2017. Uniformity optimization and dynamic studies of plasma jet array interaction in argon. Phys. Plasmas 24, 093507.

Weston, S., Coleman, C.M., Haupt, R., Logue, J., Matthews, K., Li, Y., Reyes, H.M., Weiss, S.R., Frieman, M.B., 2020. Broad anti-coronavirus activity of food and drug administration-approved drugs against SARS-CoV-2 in vitro and SARS-CoV in vivo. J. Virol. 94 (21).

Wu, H., Sun, P., Feng, H., Zhou, H., Wang, R., Liang, Y., Lu, J., Zhu, W., Zhang, J., Fang, J., 2012. Reactive oxygen species in a non-thermal plasma microjet and water system: generation, conversion, and contributions to bacteria inactivation—an analysis by electron spin resonance spectroscopy. Plasma Process Polym. 9, 417–424.

Wu, Z.G., Zheng, H.Y., Gu, J., Li, F., Lv, R.L., Deng, Y.Y., Xu, W.Z., Tong, Y.Q., 2020. Effects of different temperature and time durations of virus inactivation on results of real-time fluorescence PCR testing of COVID-19 viruses. Curr. Med. Sci. 40 (4), 614–617.

Xiling, G., Yin, C., Ling, W., Xiaosong, W., Jingjing, F., Fang, L., Xiaoyan, Z., Yiyue, G., Ying, C., Lunbiao, C., Liubo, Z., Hong, S., Yan, X., 2021. In vitro inactivation of SARS-CoV-2 by commonly used disinfection products and methods. Sci. Rep. 11 (1), 2418.

Xu, H., Zhu, Y., Du, M., Wang, Y., Ju, S., Ma, R., Jiao, Z., 2021. Subcellular mechanism of microbial inactivation during water disinfection by cold atmospheric-pressure plasma. Water Res. 188, 188.

Yamashiro, R., Misawa, T., Sakudo, A., 2018. Key role of singlet oxygen and peroxynitrite in viral RNA damage during virucidal effect of plasma torch on feline calicivirus. Sci. Rep. 8, 17947.

Yo, A., Htb, C., Mh, B., St, A., 2019. l - Dehydroascorbic acid recycled by thiols efficiently scavenges non-thermal plasma-induced hydroxyl radicals. Arch. Biochem. Biophys. 669, 87–95.

Zhang, C., Fang, Z., Liu, W., Tian, F., Bai, M., 2016. Rapid removal of bacterial endotoxin and natural organic matter in water by dielectric barrier discharge plasma: efficiency and toxicity assessment. J. Hazard. Mater. 318, 15–23.

Zhang, H., Chen, M., Huang, L., Guo, L., Xu, S., Zhang, J., Xi, W., Wang, Z., Liu, D., Kong, M.G., Rong, M., 2021. Using cold atmospheric plasma treated-air for COVID-19 disinfection in cold-chain environment. J. Phys. D. Appl. Phys. 54, 5, 40LT01.

Zhou, P., Fan, H., Lan, T., Yang, X.L., Shi, W.F., Zhang, W., Zhu, Y., Zhang, Y.W., Xie, Q. M., Mani, S., Zheng, X.S., Li, B., Li, J.M., Guo, H., Pei, G.Q., An, X.P., Chen, J.W., Zhou, L., Mai, K.J., Wu, Z.X., Li, D., Anderson, D.E., Zhang, L.B., Li, S.Y., Mi, Z.Q., He, T.T., Cong, F., Guo, P.J., Huang, R., Luo, Y., Liu, X.L., Chen, J., Huang, Y., Sun, Q., Zhang, X.L., Wang, Y.Y., Xing, S.Z., Chen, Y.S., Sun, Y., Li, J., Daszak, P., Wang, L.F., Shi, Z.L., Tong, Y.G., Ma, J.Y., 2018. Fatal swine acute diarrhoea syndrome caused by an HKU2-related coronavirus of bat origin. Nature 556, 255–258.

Zhou, P., Yang, X.L., Wang, X.G., Hu, B., Zhang, L., Zhang, W., Si, H.R., Zhu, Y., Li, B., Huang, C.L., Chen, H.D., Chen, J., Luo, Y., Guo, H., Jiang, R.D., Liu, M.Q., Chen, Y., Shen, X.R., Wang, X., Zheng, X.S., Zhao, K., Chen, Q.J., Deng, F., Liu, L.L., Yan, B., Zhan, F.X., Wang, Y.Y., Xiao, G.F., Shi, Z.L., 2020. A pneumonia outbreak associated with a new coronavirus of probable bat origin. Nature 579 (7798), 270–273.